


Constraints on the production and escape of ionizing radiation from the emission-lines of metal-poor star-forming galaxies

A. Plat¹ , S. Charlot¹, G. Bruzual², A. Feltre^{1,3,4}, A. Vidal-García^{1,5},
C. Morisset⁶ and J. Chevallard¹

¹Sorbonne Université, CNRS, UMR7095, Institut d'Astrophysique de Paris, F-75014, Paris, France

²Instituto de Radioastronomía y Astrofísica, UNAM, Campus Morelia, Michoacan, México, C.P. 58089, México

³SISSA, via Bonomea 265, I-34136 Trieste, Italy

⁴Univ. Lyon, Univ. Lyon1, ENS de Lyon, CNRS, Centre de Recherche Astrophysique de Lyon, UMR5574, 69230 Saint-Genis-Laval, France

⁵LERMA, Observatoire de Paris, Ecole Normale Supérieure, PSL Research University, CNRS, UMR8112, F-75014 Paris, France

⁶Instituto de Astronomía, UNAM, Apdo. postal 106, C.P. 22800 Ensenada, Baja California, México

Abstract. To understand how the nature of the ionizing sources and the leakage of ionizing photons in high-redshift galaxies can be constrained from their emission-line spectra, we compare emission-line models of star-forming galaxies including leakage of ionizing radiation, active galactic nuclei (AGN) and radiative shocks, with observations of galaxies at various redshifts with properties expected to approach those of primeval galaxies.

Keywords. galaxies: general, galaxies: high-redshift, galaxies: ISM

We investigate the properties of young galaxies by following the approach of Charlot & Longhetti (2001) and Gutkin *et al.* (2016) to compute the emission from star-forming galaxies, for both ionization-bounded and density-bounded models to account for the leakage of ionizing photons. We also include the emission from AGN narrow-line regions using an updated version of the Feltre *et al.* (2016) models and the emission from radiative shocks by appealing to the models of Alarie *et al.* (2019). All models are computed with the same physically-consistent description of element abundances and depletion onto dust grains. We assemble an observational sample of 68 metal-poor star-forming galaxies, 6 confirmed and 23 candidate LyC leakers and a few more quiescent star-forming galaxies and AGN, at redshifts up to 7.1. These observations are compared with the models in various diagnostic diagrams involving ultraviolet and optical emission lines. While these data had been interpreted independently in previous studies, with only a few lines typically available at once, our approach allows the simultaneous investigation of multiple diagnostics with a wide collection of homogenous models. Fig. 1 shows an example of diagram comparing this observational sample with the models, the effects of different physical parameters on emission lines being illustrated by segments of different colours. Observations are plotted in grey. The black circle corresponds to a ‘standard’ model (with constant star formation of 3 Myr, upper IMF cutoff $m_{\text{up}} = 300 M_{\odot}$, metallicity $Z = 0.002$, ionization parameter $\log \langle U \rangle = -2$, gas density $n_{\text{H}} = 10^2 \text{ cm}^{-3}$, dust-to-metal

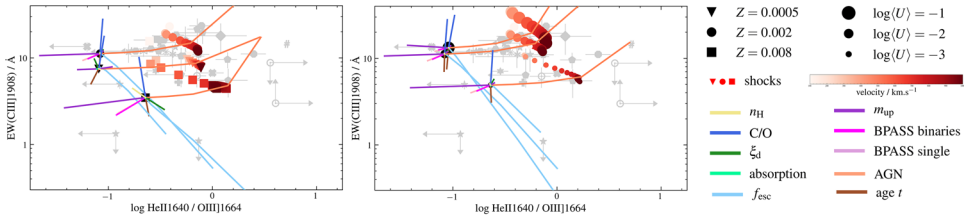


Figure 1. Segments of different colours show the effect of altering a single parameter at the time with respect to the standard model: rise in C/O ratio from 0.17 to $(C/O)_{\odot} = 0.44$ (blue); drop in dust-to-mass ratio from $\xi_d = 0.3$ to 0.1 (dark green); rise in n_H from 10^2 to 10^3 cm^{-3} (yellow); inclusion of interstellar-line absorption in the H II interiors and outer H I envelopes of stellar birth clouds (light green); increase in stellar population age from 3 to 10 Myr (brown); rise in m_{up} from 100, to 300, to $600 M_{\odot}$ (dark purple); adopting the BPASS single- (light purple) and binary-star (magenta) models in place of the C&B model (BPASS models are not available for $Z = 0.0005$); drop in the optical depth to LyC photons at 570 \AA from +1.0 to -1.0 (light blue); inclusion of an AGN component contributing from 0 to over 90% of the total He II $\lambda 1640$ emission (orange); and inclusion of a radiative-shock component contributing 90% of the total He II $\lambda 1640$ emission [red symbols, with shape corresponding to the metallicity of the associated benchmark model, and darkness to the shock velocity, from 10^2 km s^{-1} (light) to 10^3 km s^{-1} (dark)]. See Plat *et al.* (2019) for details.

mass ratio $\xi_d = 0.3$, C/O ratio of 0.17), while the black upside-down triangle and black square are benchmark models with the same parameters, but with $Z = 0.0005$ and 0.008, respectively, and the different sizes correspond to different ionization parameters.

From this analysis, we confirm that models of star-forming galaxies powered by either single-star population (as in the latest version of the Bruzual & Charlot (2003) model) or binary-star population (as in the latest version of the Eldridge *et al.* (2017) models) overall reproduce the observed emission-line properties of young metal-poor star-forming galaxies, except in diagrams involving He II ($\lambda 1640$ and $\lambda 4686$) recombination lines. The models can be brought into agreement with the observations in all line-ratio diagrams by invoking an AGN or a radiative-shock component, which increases He II emission and the line equivalent width (see, e.g., Fig. 1). We also confirm that, while a rise in the escape fraction of Lyman continuum photons in density-bounded models triggers a drop in the equivalent widths of low-ionization potential lines, and in the ratios of low- to high-ionization potential lines, these signatures are degenerate with several other parameters, such as the nature of the ionizing source, the age of the stellar population, the metallicity and ionization parameter of interstellar gas, in such a way that most regions of ultraviolet and optical line-ratio diagrams sampled by observations can be covered by both ionization-bounded and density-bounded photoionization models. Hence, firm conclusions about the escape of LyC photons cannot be drawn without detailed comparisons of models with observations in several diagnostic diagrams at once.

References

- Alarie, A. S., Morisset, C., & Binette, L. 2019, *Rev. Mex. Astron. Astrofis.*, submitted
- Bruzual, G. & Charlot, S. 2003, *MNRAS*, 344, 1000
- Charlot, S. & Longhetti, M. 2001, *MNRAS*, 323, 887
- Eldridge, J. J., Stanway, E. R., Xiao, L., McClelland, L. A. S., Taylor, G., Ng, M., Greis, S. M. L., & Bray, J. C. 2017, *Publ. Astron. Soc. Australia*, 34, e058
- Feltre, A., Charlot, S., & Gutkin J. 2016, *MNRAS*, 462, 1757
- Gutkin, J., Charlot, S., & Bruzual, G. 2016, *MNRAS*, 462, 1757
- Vidal-Garc'a, A., Charlot, S., Bruzual, G., & Hubeny, I. 2017, *MNRAS*, 470, 3532